Focal adhesion kinase antagonizes doxorubicin cardiotoxicity via p21^{Cip1}

SUPPLEMENTAL MATERIAL

Cheng et al.

Supplemental Information includes Supplemental Methods, eight figures with legends, Supplemental Discussion, and Supplemental References.

Supplemental Methods

Generation of knockout and transgenic mice. Myocyte-restricted FAK knockout (MFKO) and cardiac-specific SuperFAK (SF) transgenic mice (SF2) were generated as described previously [1, 2]. In brief, *mlc2v-cre* $^{+/-}$ mice (kindly provided by Dr. Kenneth Chien, Harvard Medical School) were crossed to and *fak*$^{+/-}$ mice to obtain *mlc2v-cre*$^{+/-}$/*fak*$^{+/-}$ mice, which were then crossed with *fak*$^{flox/flox}$ mice (graciously provided by Drs. Louis Reichardt and Hilary Beggs, University of California, San Francisco) to generate *mlc2v-cre*$^{+/-}$/*fak*$^{flox/-}$ (MFKO) mice. SF2 mice were generated by standard transgenic approaches using a construct containing a 3.4-kb rat cardiac beta myosin heavy chain (β-MHC) promoter fragment upstream of the SuperFAK cDNA (kindly provided by Dr. Michael Schaller, West Virginia University).

Echocardiography. Left ventricular function was measured by 2D echocardiography in conscious mice using the Visualsonic Ultrasound System (Vevo 660) with a 30 MHz high-frequency transducer as described previously[2]. Echocardiographic measurements from more than three consecutive cycles were averaged using the Visual Sonics software.

Primary cardiomyocyte isolation. Primary cardiomyocytes were isolated from 2- to 3-day-old Wistar rats or as indicated using the Neonatal Cardiomyocyte Isolation System (Worthington Biochemical Corporation, NJ). Hearts were minced in Ca^{2+} and Mg^{2+} -free Hank's balanced salt solution, digested with 50μg/ml trypsin at 4°C overnight followed by 100U/ml collagenase at 37°C for 45min. Neonatal rat cardiomyocytes (NRCMs) were released and plated on fibronectin-coated plastic or glass surfaces in Media 199 supplemented with 15%FBS, 1% penicillin/streptomycin in the presence of 100 μM BrdU to eliminate proliferating nonmyocytes. 24h later, cells were washed with PBS twice and cultured in serum-free Media 199 followed by transfection or infections.

Adenoviral infection and siRNA transfection. NRCMs were infected with GFP, SF, LacZ, or p21 adenoviruses at a multiplicity of infection (MOI) of 50 or as indicated. Transfection of NRCMs with siRNA (25nM) was performed using the HiPerfect transfection reagent (Qiagen) according to the manufacturer's instructions. Specific siRNAs for rat p21 (sc-108036) and FAK (sc-156037) were obtained from Santa Cruz Biotechnology; The control scrambled siRNA was obtained from Invitrogen.

Subcellular fractionation. Hearts or NRCMs were homogenized in ice-cold isolation buffer (70mM sucrose, 190mM D-Mannitol, 20mM Hepes, 0.2mM EDTA) as described previously[3]. Nuclei were pelleted by centrifugation at 600g for 10min and extracted with RIPA buffer. Mitochondrial fraction were separated by centrifugation of the supernatant at 5000g for 15 min. Cytosolic fraction were obtained by re-centrifugation of the supernatant at 20,000g for 60min.

Western blotting. Protein lysates were electrophoresed through SDS-polyacrylamide gels and transferred to PVDF membranes. The following antibodies were used: mouse anti-p21 (556431, BD Biosciences, 1:1000), rabbit anti-pFAK (Y397) (44624G, Invitrogen, 1:1000), mouse anti-FAK (clone 4.47, Millipore, 1:1000), rabbit anti-caspase 3 (#9662, Cell signaling, 1:500), rabbit anti-PARP (#9542, Cell signaling, 1:500), rabbit anti-Histone H3 (ab1791, Abcam, 1:1000) and rabbit anti-GAPDH (sc-25778, Santa Cruz Biotechnology, 1:1000).

Immunofluorescence and TUNEL staining. Paraffin sections were treated for antigen retrieval using 10 mmol/L citrate buffer (pH 6.0). Primary cultured cardiomyocytes were permeabilized with fresh permeabilization solution (0.1%Triton X-100 and 0.1% sodium citrate in PBS). Slides were incubated with anti-cardiac Troponin T (Thermo scientific) at 4°C overnight to label cardiomyocytes.

For TUNEL assay, sections were incubated with the TUNEL reaction mixture for 1 hr at 37°C using the In Situ Cell Death Detection Kit (Roche Applied Science). Fluorescence images were obtained using a Zeiss LSM 710 confocal laser-scanning microscope (Zeiss, Germany).

Cell viability assay. Cell viability was assessed by using the MTT assay kit (Roche) or the Live/Dead viability/cytotoxicity kit (Invitrogen). For MTT assay, NRCMs were plated at 50,000 cells/well in a 96 well plate and infected with indicated adenoviruses at MOI 50. 48 hrs later, cells were treated with vehicle or DOX (1μM) for 24 hrs. After incubation with 0.5mg/ml MTT labeling reagent for 4 hrs, formazan crystals were dissolved by addition of 100μL Solubilization solution and incubation for another 16 hrs. Absorbance at 562 nm were measured by using a microplate reader. For the Live/Dead viability assay, cells were incubated with 2 μM calcein AM and 4 μM Ethidium homodimer-1 for 45 min at room temperature. Cell viability was evaluated according to the manufacturer's instructions.

RT-PCR. Total RNA was extracted from cultured cardiomyocytes using the RNeasy kit (Qiagen). 500ng of total RNA was reverse-transcribed into cDNA by using the iScript cDNA synthesis kit (Bio-Rad). 50ng cDNA was subjected to semi-quantitative PCR reactions using the following programs: (25 cycles) 94˚C 30s, 55˚C 30s, 72˚C 20s for p21 and GAPDH; (26 cycles) 94˚C 30s, 56˚C 30s, 72˚C 20s for Bim. Primer pairs used were as follows: p21, 5'-TTGTCGCTGTCTTGCACTCTG-3' and 5'-GCGCTTGGAGTGATAGAAATCTG-3'; GAPDH, 5'-AAGGTCGGTGTGAACGGATTTG-3' and 5'-CCTTCTCCATGGTGGTGAAGAC-3'; Bim, 5'-CCATGAGTTGTGACAAGTCAACAC-3' and 5'-GATCTTCAGGTTCCTCCTGAGACTG-3'.

Assessment of ΔΨm. Mitochondrial membrane potential (ΔΨm) was measured by confocal microscopy using the JC-1 mitochondrial membrane potential assay kit (Cayman Chemical). NRCMs were incubated with JC-1 for 30 min at 37°C and examined with a 10X objective lens. JC-1 forms J-aggregates (red) in healthy cells with high ΔΨm and exists as monomers (green) in apoptotic cells with low ΔΨm. Loss of ΔΨ is visualized by a shift from red to green fluorescence. Integrated density of fluorescence was measured using the Image J software (NIH) and the ratio of JC-1 monomers to J-aggregates was analyzed as an index of mitochondrial membrane depolarization.

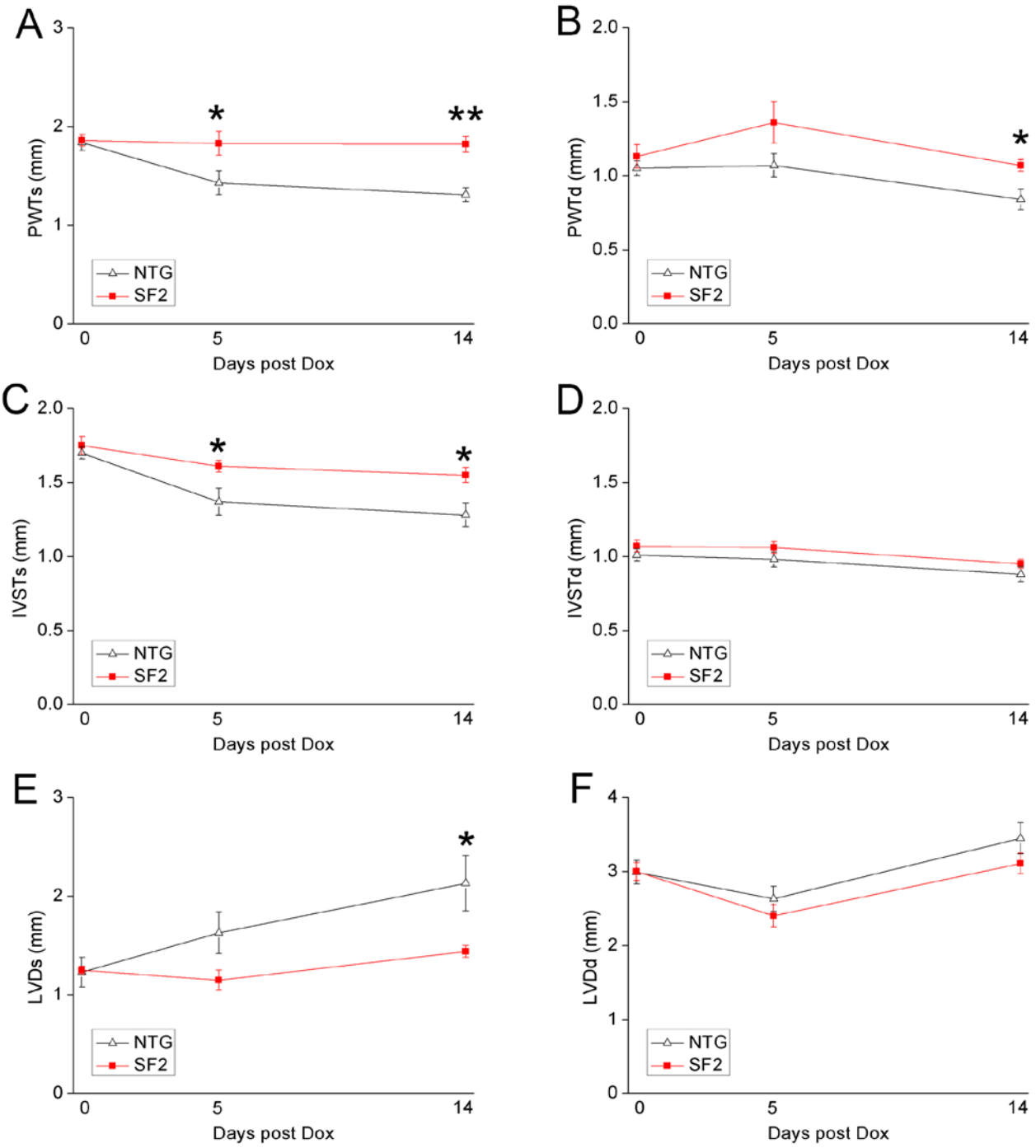

Supplemental Figure 1. Echocardiographic assessment of cardiac function in NTG and SF2 mice treated with DOX (20mg/kg, i.p. n=8 per group). (**A**) PWTs, left ventricular posterior wall thickness at end systole. (**B**) PWTd, left ventricular posterior wall thickness at end diastole. (**C**) IVSTs, interventricular septal thickness at end systole (IVSTs). (**D**) IVSTd, interventricular septal thickness at end diastole. (**E**) LVDs, left ventricular diameter at end systole. (**F**) LVDd, left ventricular diameter at end diastole. * *P*<0.05; ** *P*<0.01 vs. NTG. Data are mean ± SEM.

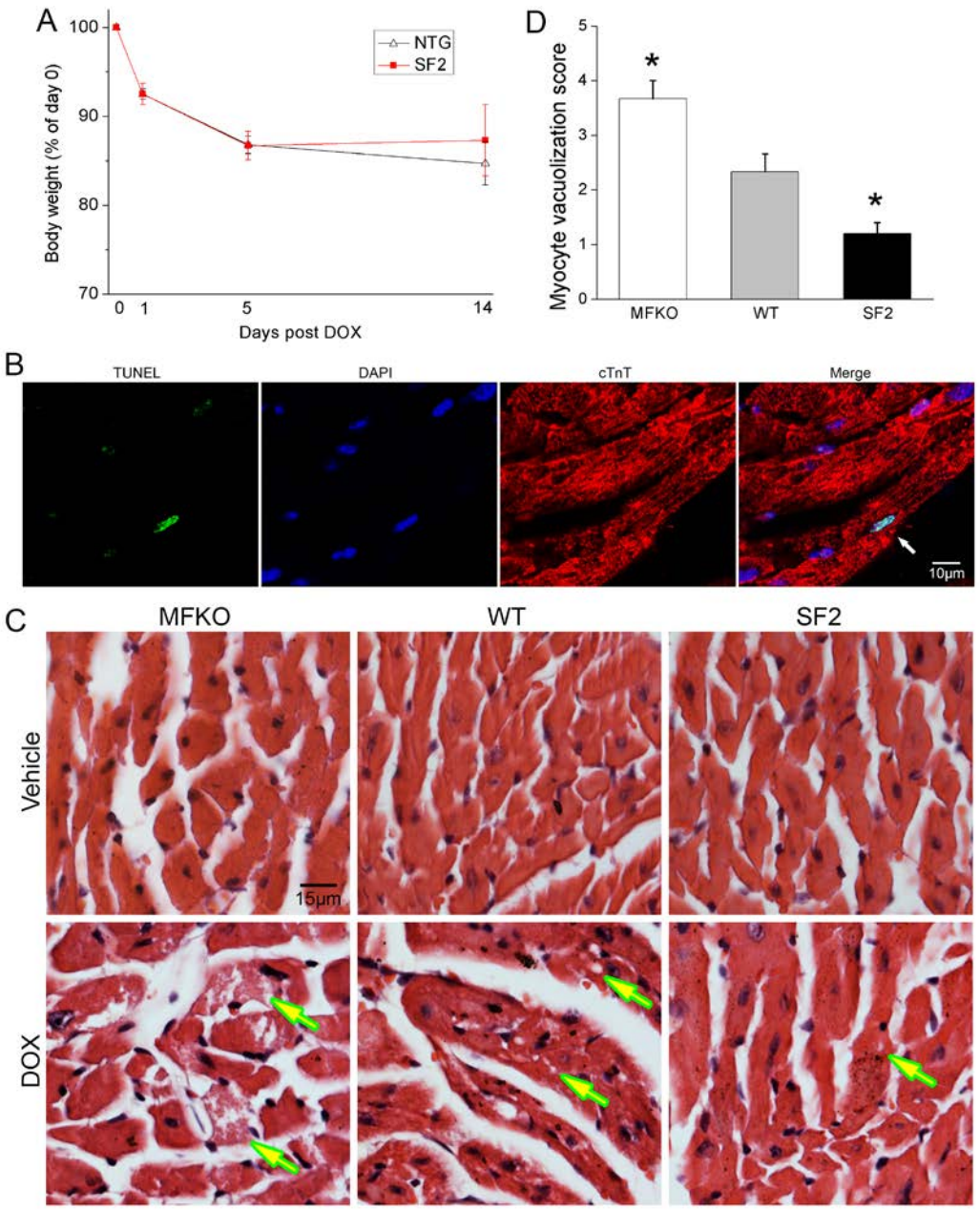

Supplemental Figure 2. FAK antagonizes cardiac toxicity induced by doxorubicin (DOX). (**A**) DOX-induced comparable body weight loss in NTG and SF2 mice. SF2(n=8) and NTG (n=8) received a single injection of DOX (20mg/kg, i.p.). Values are expressed as percentage of baseline body weight for each mouse. Data are mean ± SEM. (**B**) Representative image of apoptotic cardiomyocyte in NTG heart following 1 day of DOX treatment. Apoptosis was assessed by TUNEL staining (*green*, Arrow). Nuclei were stained with DAPI (*blue*) and cardiomyocytes were stained with cardiac troponin T (cTnT, *red*). Scale bar =10μm. (**C**) Heart sections from DOX or vehicle-treated mice 5 days after injection were stained with hematoxylin & eosin. Myocyte vacuolization and myofibrillar loss were indicated by arrows. Images are representative of 5 to 9 mice/group. (**D**) Quantification of myocyte vacuolization and myofibrillar loss from at least 200 cells per heart was performed as described previously [4] (Grading score system: 1, Minimal; 2, Mild; 3, Moderate; and 4, Marked). * *P*<0.05 vs. WT.

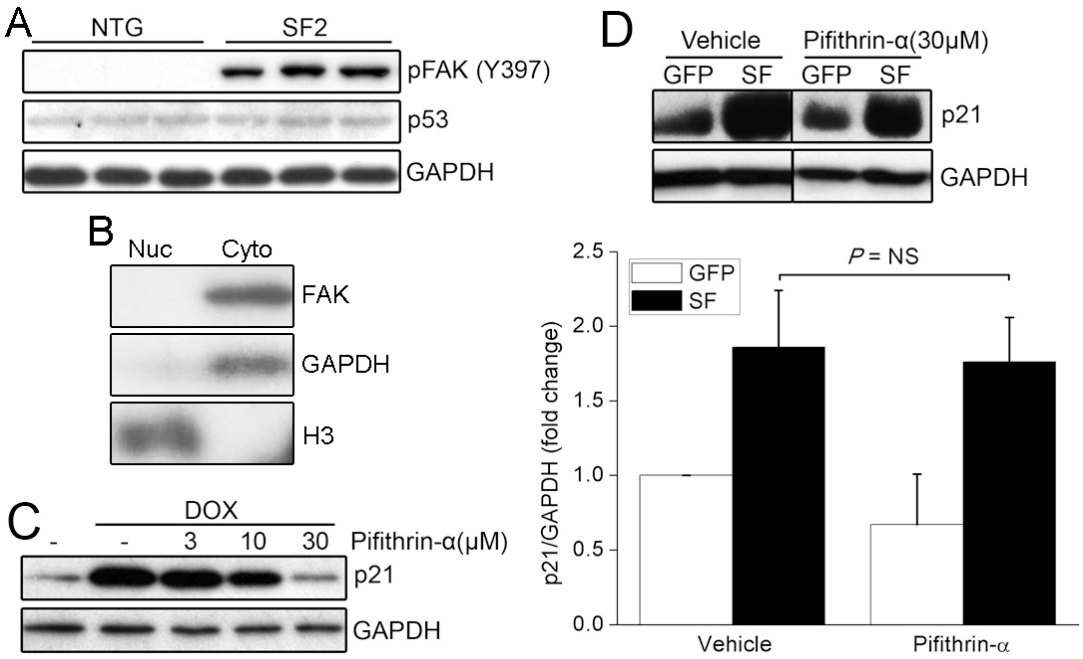

Supplemental Figure 3. FAK-induced p21 expression is independent of p53. (**A**)Protein levels of p53 were comparable between NTG and SF2 hearts at day 14 post DOX injection (20mg/kg, i.p.), suggesting myocardial FAK activation did not induce p53 degradation. (**B**) Cytoplasmic localization of FAK in adult mouse heart. Subcellular fractionation was performed in adult mouse heart. Nuclear (Nuc) and Cytosolic (Cyto) fractions were subjected to Western blotting using indicated antibodies. Histone H3 served as a nuclear loading control and GAPDH as a cytosolic loading control. (**C**) NRCMs were treated with DOX (1μM) for 4hrs in the presence of various concentrations of pifithrin-α, a p53 inhibitor. Treatment with pifithrin-α (30 μM) completely blocked DOX-induced (p53-dependent) p21 expression. (**D**) NRCMs were infected with GFP or SF adenoviruses prior to incubation with pifithrin-α (30 μM) for 24hrs. Treatment with pifithrin-α did not alter SF-mediated up-regulation of p21. Results are mean±SEM of 3 independent experiments.

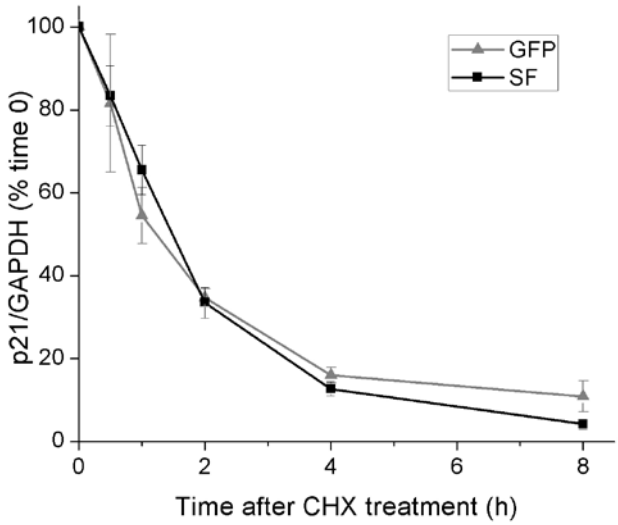

Supplemental Figure 4. Activation of FAK did not alter p21 protein stability. NRCMs were infected with GFP or SF adenoviruses prior to incubation with the protein synthesis inhibitor cycloheximide (CHX, 10μg/ml) for various periods of time. Graph shown is quantification of Western blot performed in Figure 3E. Data are mean±SEM of 3 independent experiments.

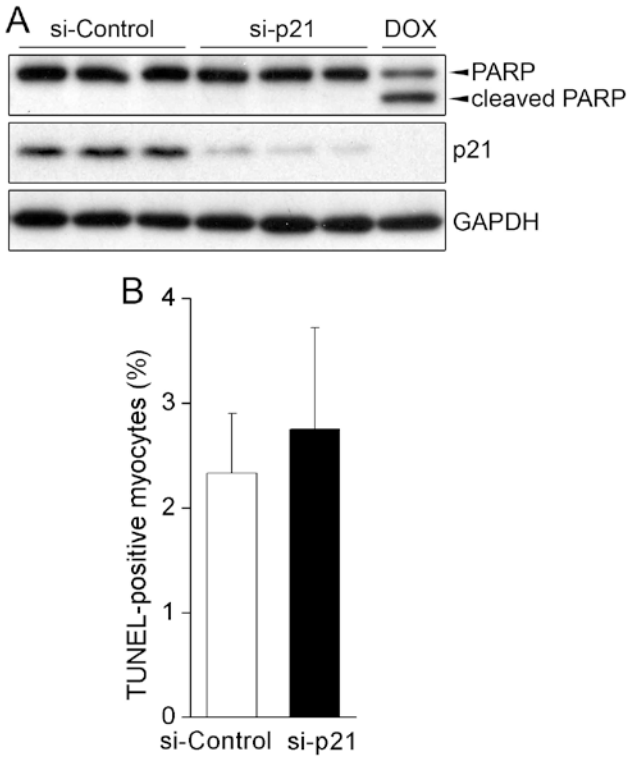

Supplemental Figure 5. Knockdown of p21 alone did not influence basal cardiomyocyte survival. NRCM were transfected with si-Control or si-p21. (**A**) Western blotting revealed that depletion of p21 did not induce PARP cleavage. DOX-treated NRCM served as positive control. (**B**) Quantification of TUNEL-positive myocytes. Knockdown of p21 did not significantly enhance TUNEL labeling. Data are mean±SEM of 4 independent experiments.

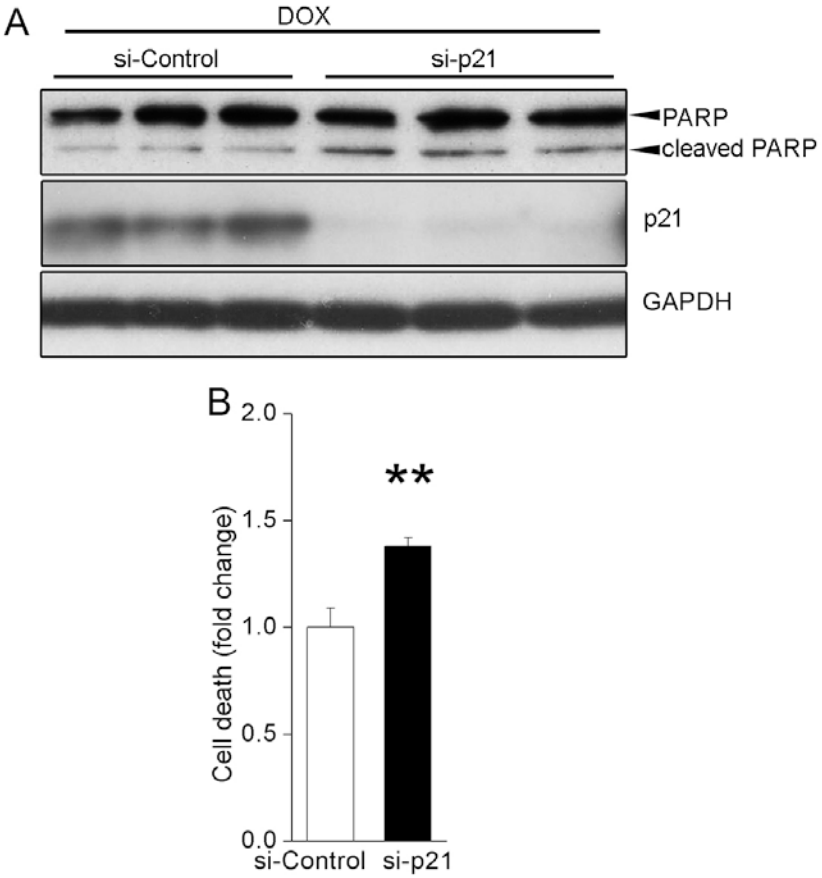

Supplemental Figure 6. Silencing of p21 promoted DOX sensitivity in terminally differentiated cardiomyocytes. Primary cardiomyocytes were isolated from 10-day-old rats and transfected with si-Control or si-p21 in serum-free media. (**A**) Western blotting of cells treated with DOX (1 μM) for 24h revealed that depletion of p21 enhanced PARP cleavage induced by DOX. GAPDH served as a loading control. (**B**) Cell viability was assessed by staining with calcein AM/Ethidium homodimer-1 as described in the Methods. Knockdown of p21 exaggerated cell death induced by DOX. Data are mean±SEM of 4 independent experiments.

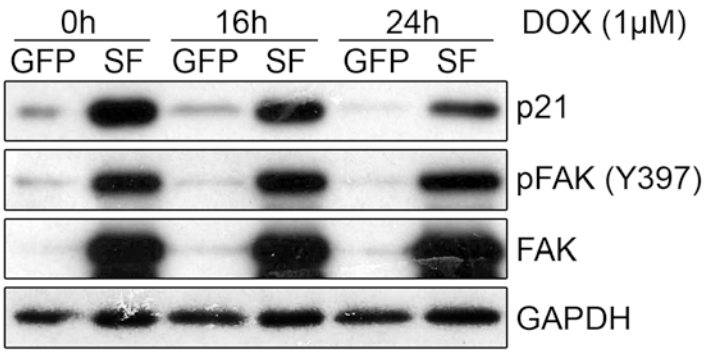

Supplemental Figure 7. SuperFAK expressing cardiomyocytes maintained higher levels of p21 following DOX treatment than GFP-expressing controls. NRCMs were infected with GFP or SF adenoviruses at 50 MOI. 24 hr later, cells were treated with DOX (1μM) for the indicated times and p21 levels were detected by Western blotting. GAPDH is shown as a loading control. The images are representative of 3 independent experiments.

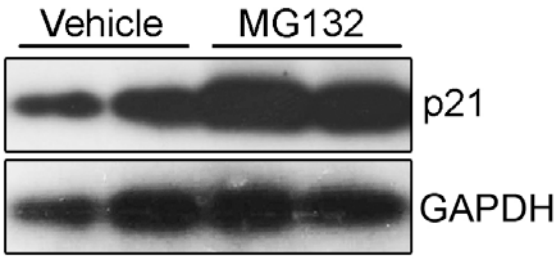

Supplemental Figure 8. Proteasomal degradation of p21 in cardiomyocytes under basal conditions. NRCMs were treated with the 26S proteasome inhibitor MG132 (10μM) for 16h. Inhibition of the proteasome blocked basal p21 degradation in cardiomyocytes.

Supplemental Discussion

In the present study, we demonstrated that FAK antagonizes DOX cardiotoxicity via up-regulation of p21 mRNA. Interestingly, the sphingosine kinase/sphingosine 1-phosphate axis, which induces phosphorylation and activation of FAK [5], is also involved in p21 induction and resistance to DOX cytotoxicity [6, 7]. Moreover, several other growth factors that act upstream of FAK including epidermal growth factor [8], fibroblast growth factor [9], and platelet-derived growth factor [10] also up-regulate p21. It is well known that p21 levels are tightly controlled by extensive regulation at both the transcriptional and post-transcriptional level. While overexpression of FAK-related nonkinase (FRNK), an endogenous FAK inhibitor, was reported to increase the protein stability of p21, this was found to be accompanied by a ~40% reduction in p21 mRNA levels [11]. Our data extend these findings and support a post-transcriptional mechanism for FAK-dependent maintenance of elevated p21 mRNA. p21 contains several conserved RNA binding protein motifs within the 3'UTR of the gene and association of the RNA binding proteins from the RNPE family, HuR, KSRP and FXR1P have been shown to regulate p21 mRNA stability[12-17]. Whether FAK activity modulates the binding of these regulators or influences the recruitment of bone fide p21 microRNAs (such as miR-22 [18]) are interesting questions for future studies.

In contrast, treatment with DOX induced degradation of p21 through the ubiquitin-proteasome pathway. It is presently unclear which E3 ligase targets myocardial p21 for degradation following DOX treatment. p21 is a short-lived protein and at least 6 different E3 ligases can promote its ubiquitination and degradation [19, 20]. These various E3 ligases target different sub-pools of p21 and the specificity of these interactions is conferred by p21 binding proteins (for example the E3 ligase Cdt2 only targets p21 for degradation when p21 is bound to PCNA and loaded onto chromatin). It will be of future interest to explore whether E3 ligases reported to induce p21 degradation following UV-induced DNA damage (Skp2, p53RFP or MKR1 [37]) play a role in DOX-dependent p21 degradation or whether the more recently discovered cullin, CRL2 that induces degradation of cytoplasmic p21 is involved [21].

We also showed that cardiac p21 suppressed expression of the pro-apoptotic BH3-only protein Bim. However, we cannot rule out additional protective mechanism(s) that could result from the capacity of p21 to interact with and directly inhibit downstream execution molecules such as procaspase-3 [22] and apoptosis signal-regulating kinase-1[23] mechanisms that have been implicated p21-dependent survival of other cell types. It is interesting to note that the cardioprotective effect of pro-survival signaling through Pim-1 and AKT has been reported to be mediated, at least in part, by promoting mitochondrial integrity [24, 25] and p21 is a substrate for both of these kinases [26, 27]. Indeed, activation of Akt/Pim-1 signaling can enhance the stabilization and cytoplasmic accumulation of p21. Thus it will be of future interest to determine the extent to which the anti-apoptotic effects of these kinases can be attributed to altered p21stability/locale.

Supplemental References

[1] DiMichele LA, Doherty JT, Rojas M, Beggs HE, Reichardt LF, Mack CP, et al. Myocyte-restricted focal adhesion kinase deletion attenuates pressure overload-induced hypertrophy. Circ Res. 2006;99:636-45.

[2] Cheng Z, DiMichele LA, Hakim ZS, Rojas M, Mack CP, Taylor JM. Targeted focal adhesion kinase activation in cardiomyocytes protects the heart from ischemia/reperfusion injury. Arterioscler Thromb Vasc Biol. 2012;32:924-33.

[3] Cheng Z, Volkers M, Din S, Avitabile D, Khan M, Gude N, et al. Mitochondrial translocation of Nur77 mediates cardiomyocyte apoptosis. Eur Heart J. 2011;32:2179-88.

[4] Vacchi-Suzzi C, Bauer Y, Berridge BR, Bongiovanni S, Gerrish K, Hamadeh HK, et al. Perturbation of microRNAs in rat heart during chronic doxorubicin treatment. PLoS One. 2012;7:e40395.

[5] Wang F, Nobes CD, Hall A, Spiegel S. Sphingosine 1-phosphate stimulates rho-mediated tyrosine phosphorylation of focal adhesion kinase and paxillin in Swiss 3T3 fibroblasts. Biochem J. 1997;324 (Pt 2):481-8.

[6] Sankala HM, Hait NC, Paugh SW, Shida D, Lepine S, Elmore LW, et al. Involvement of sphingosine kinase 2 in p53-independent induction of p21 by the chemotherapeutic drug doxorubicin. Cancer Res. 2007;67:10466-74.

[7] Huwiler A, Kotelevets N, Xin CY, Pastukhov O, Pfeilschifter J, Zangemeister-Wittke U. Loss of sphingosine kinase-1 in carcinoma cells increases formation of reactive oxygen species and sensitivity to doxorubicin-induced DNA damage. Brit J Pharmacol. 2011;162:532-43.

[8] Ruddel J, Wennekes VE, Meissner W, Werner JA, Mandic R. EGF-dependent induction of BCL-xL and p21CIP1/WAF1 is highly variable in HNSCC cells--implications for EGFR-targeted therapies. Anticancer Res. 2010;30:4579-85.

[9] Aikawa T, Segre GV, Lee K. Fibroblast growth factor inhibits chondrocytic growth through induction of p21 and subsequent inactivation of cyclin E-Cdk2. J Biol Chem. 2001;276:29347-52.

[10] Moon SK, Jung SY, Choi YH, Lee YC, Kim CH. Platelet-derived growth factor induces p21/WAF1 promoter in vascular smooth muscle cells via activation of an Sp1 site. FEBS Lett. 2003;552:130-4.

[11] Bryant P, Zheng Q, Pumiglia K. Focal adhesion kinase controls cellular levels of p27/Kip1 and p21/Cip1 through Skp2-dependent and -independent mechanisms. Mol Cell Biol. 2006;26:4201-13.

[12] van der Giessen K, Di-Marco S, Clair E, Gallouzi IE. RNAi-mediated HuR depletion leads to the inhibition of muscle cell differentiation. J Biol Chem. 2003;278:47119-28.

[13] Davidovic L, Durand N, Khalfallah O, Tabet R, Barbry P, Mari B, et al. A novel role for the RNA-binding protein FXR1P in myoblasts cell-cycle progression by modulating p21/Cdkn1a/Cip1/Waf1 mRNA stability. PLoS Genet. 2013;9:e1003367.

[14] Cho SJ, Zhang J, Chen X. RNPC1 modulates the RNA-binding activity of, and cooperates with, HuR to regulate p21 mRNA stability. Nucleic Acids Res. 2010;38:2256-67.

[15] Briata P, Forcales SV, Ponassi M, Corte G, Chen CY, Karin M, et al. p38-dependent phosphorylation of the mRNA decay-promoting factor KSRP controls the stability of select myogenic transcripts. Mol Cell. 2005;20:891-903.

[16] Waggoner SA, Johannes GJ, Liebhaber SA. Depletion of the poly(C)-binding proteins alphaCP1 and alphaCP2 from K562 cells leads to p53-independent induction of cyclin-dependent kinase inhibitor (CDKN1A) and G1 arrest. J Biol Chem. 2009;284:9039-49.

[17] Scoumanne A, Cho SJ, Zhang J, Chen X. The cyclin-dependent kinase inhibitor p21 is regulated by RNA-binding protein PCBP4 via mRNA stability. Nucleic Acids Res. 2011;39:213-24.

[18] Tsuchiya N, Izumiya M, Ogata-Kawata H, Okamoto K, Fujiwara Y, Nakai M, et al. Tumor suppressor miR-22 determines p53-dependent cellular fate through post-transcriptional regulation of p21. Cancer Res. 2011;71:4628-39.
[19] Xiong Y. Targeting p21 degradation locally. Dev Cell. 2010;19:641-3.
[20] Starostina NG, Kipreos ET. Multiple degradation pathways regulate versatile CIP/KIP CDK inhibitors. Trends Cell Biol. 2012;22:33-41.
[21] Starostina NG, Simpliciano JM, McGuirk MA, Kipreos ET. CRL2(LRR-1) targets a CDK inhibitor for cell cycle control in C. elegans and actin-based motility regulation in human cells. Dev Cell. 2010;19:753-64.
[22] Suzuki A, Ito T, Kawano H, Hayashida M, Hayasaki Y, Tsutomi Y, et al. Survivin initiates procaspase 3/p21 complex formation as a result of interaction with Cdk4 to resist Fas-mediated cell death. Oncogene. 2000;19:1346-53.
[23] Zhan J, Easton JB, Huang S, Mishra A, Xiao L, Lacy ER, et al. Negative regulation of ASK1 by p21Cip1 involves a small domain that includes Serine 98 that is phosphorylated by ASK1 in vivo. Mol Cell Biol. 2007;27:3530-41.
[24] Muraski JA, Rota M, Misao Y, Fransioli J, Cottage C, Gude N, et al. Pim-1 regulates cardiomyocyte survival downstream of Akt. Nat Med. 2007;13:1467-75.
[25] Borillo GA, Mason M, Quijada P, Volkers M, Cottage C, McGregor M, et al. Pim-1 kinase protects mitochondrial integrity in cardiomyocytes. Circ Res. 2010;106:1265-74.
[26] Zhou BP, Liao Y, Xia W, Spohn B, Lee MH, Hung MC. Cytoplasmic localization of p21Cip1/WAF1 by Akt-induced phosphorylation in HER-2/neu-overexpressing cells. Nat Cell Biol. 2001;3:245-52.
[27] Zhang Y, Wang Z, Magnuson NS. Pim-1 kinase-dependent phosphorylation of p21Cip1/WAF1 regulates its stability and cellular localization in H1299 cells. Mol Cancer Res. 2007;5:909-22.